15 (2023) 200259

Contents lists available at ScienceDirect

Tumour Virus Research

journal homepage: www.journals.elsevier.com/tumour-virus-research

# Elevated iNOS and 3′-nitrotyrosine in Kaposi's Sarcoma tumors and mouse model

Olga Vladimirova [a], Samantha Soldan [a], Chenhe Su [a], Andrew Kossenkov [a], Owen Ngalamika [b], For Yue Tso [c], John T. West [c], Charles Wood [c], Paul M. Lieberman [a,*]

[a] The Wistar Institute, Philadelphia, PA, 19104, USA
[b] Dermatology and Venereology Section, University Teaching Hospitals, University of Zambia School of Medicine, Lusaka, P.O. Box 50110, Zambia
[c] Department of Interdisciplinary Oncology, Stanley S Scott Cancer Center, State University Health Sciences Center, New Orleans, LA, USA

ARTICLE INFO

*Keywords:*
Kaposi's Sarcoma
Kaposi's Sarcoma associated herpesvirus
HHV8
iNOS
Nitrotyrosine
L-NMMA
LANA

ABSTRACT

Kaposi's Sarcoma (KS) is a heterogenous, multifocal vascular malignancy caused by the human herpesvirus 8 (HHV8), also known as Kaposi's Sarcoma-Associated Herpesvirus (KSHV). Here, we show that KS lesions express iNOS/NOS2 broadly throughout KS lesions, with enrichment in LANA positive spindle cells. The iNOS byproduct 3-nitrotyrosine is also enriched in LANA positive tumor cells and colocalizes with a fraction of LANA-nuclear bodies. We show that iNOS is highly expressed in the L1T3/mSLK tumor model of KS. iNOS expression correlated with KSHV lytic cycle gene expression, which was elevated in late-stage tumors (>4 weeks) but to a lesser degree in early stage (1 week) xenografts. Further, we show that L1T3/mSLK tumor growth is sensitive to an inhibitor of nitric oxide, L-NMMA. L-NMMA treatment reduced KSHV gene expression and perturbed cellular gene pathways relating to oxidative phosphorylation and mitochondrial dysfunction. These finding suggest that iNOS is expressed in KSHV infected endothelial-transformed tumor cells in KS, that iNOS expression depends on tumor microenvironment stress conditions, and that iNOS enzymatic activity contributes to KS tumor growth.

## 1. Introduction

Kaposi's Sarcoma (KS) is a heterogenous, multicentric vascular tumor caused by the human herpesvirus 8 (HHV-8) also known as KS-Associated Herpesvirus (KSHV) [1–3]. KS occurs most frequently and aggressively in the context of HIV-coinfection and immunosuppression, often involving multiple organs, especially skin, lymph nodes, and oral cavity, but can also involve GI tract and internal organs [4]. KSHV can also cause pleural effusion lymphoma (PEL) and multicentric Castleman Disease (MCD).

The mechanism through which KSHV causes various cancers is not fully understood. KSHV genomes persist in PEL and KS tumor cells as multicopy episomes where a restricted subset of viral genes are expressed. Numerous viral genes have been demonstrated to have oncogenic activities, including the Latency-Associated Nuclear Antigen (LANA) −1 protein that functions to maintain the viral episome during latent infection, as well as modulate host cell gene expression and chromatin biology. KS occurs at much greater frequency in some endemic populations, especially sub-Saharan Africa and in the context of HIV-AIDS. The genetic and environmental factors that contribute to this increased incidence are only partly understood, but immune system alterations are thought to be a major contributing factor.

Numerous signaling pathways have been implicated in the pathogenesis of KS. Recent RNA-seq transcriptomics identified glucose and lipid metabolism pathway disruption in KS tumors relative to healthy controls [5,6]. Significant perturbations in interferon inducible and inflammatory cytokine pathway genes were also upregulated in KS, along with regulators of angiogenesis and epithelial-mesenchymal transition (EMT). Many of these features have also been recapitulated in cell culture models of KSHV infection, although no single cell culture model completely recapitulates all features observed in KS. This may partly be due to the heterogeneity of KS tumor cells and subtypes. Consequently, a major challenge in the field is developing suitable cell culture or animal models to study KS tumorigenesis.

One of the highly significant cellular genes upregulated in KS tumors was NOS2, also known as iNOS [5,6]. Early studies identified iNOS expression in KS lesions and concluded the expression was associated with vascular endothelial cells and infiltrating macrophages [7]. More recent studies have shown that iNOS is upregulated in KSHV

* Corresponding author.
*E-mail address:* Lieberman@wistar.org (P.M. Lieberman).

https://doi.org/10.1016/j.tvr.2023.200259
Received 18 September 2022; Received in revised form 24 January 2023; Accepted 20 February 2023
Available online 1 March 2023
2666-6790/© 2023 The Authors. Published by Elsevier B.V. This is an open access article under the CC BY-NC-ND license (http://creativecommons.org/licenses/by-nc-nd/4.0/).

**Abbreviations**

| | |
|---|---|
| KSHV | Kaposi's Sarcoma-Associated Herpesvirus |
| iNOS | inducible nitric oxide synthase (NOS2) |
| L-NMMA | $N^G$-methyl L-arginine |
| PEL | Pleural Effusion Lymphoma |
| MCD | Multicentric Castleman Disease |
| GI | gastrointestinal |
| LANA | Latency Associated Nuclear Antigen |
| LANA-NBs | Latency Associated Nuclear Antigen Nuclear Bodies |
| VEGF | Vascular Endothelial Growth Factor |
| FFPE | Formaldehyde Fixed Parafin Embedded |
| FDR | false-discovery rate |
| IHC | Immunohistochemistry |
| IF | immunofluorescence |
| SLK | Caki-1 cell line |
| HUVEC | human vascular endothelial cells |
| LECs | lymphatic endothelial cells |
| MSCs | mesenchymal stem cells |
| TIVE | telomerase immortalized vascular endothelial cells |
| STR | short tandem repeats |

transformed rat embryonic metanephric mesenchymal cells (KMM) models of KS [8]. In this model, siRNA depletion of iNOS inhibited production of nitric oxide (NO), inflammatory signaling through STAT3, and oncogenic cell phenotype. iNOS can be expressed at very high levels to produce transient bursts of NO, a free-radical signaling molecule involved in diverse cellular processes and implicated in pathogenesis of various disease, including cancer [9]. iNOS and high-levels of NO have a well-established role in the anti-microbial activities of macrophages [10]. However, iNOS has also been found expressed in endothelial cells and various tumor types [9,10]. Chronic NO production can function as a genotoxic and reactive radical that can drive cancer cell progression [11]. NO produced by tumor cells can also activate VEGF and induce pro-angiogenic activity [12]. NO is also known to play a central role in how cells respond to hypoxia [13]. Therefore, how NO contributes to KS remains an important unanswered question.

## 2. Materials & methods

### 2.1. KS tumor samples

All KS tumors samples formalin-fixed paraffin embedded blocks and slide were deidentified and from a Zambian KS cohort. A description of the study cohort and ethics review have been published previously [5, 6].

### 2.2. Cell lines

iSLK cells (gift from Don Ganem, Novartis) [14] were cultured in Dulbecco's Modified Eagle's medium (DMEM) supplemented with 10% fetal bovine serum (FBS, heat inactivated) and 1% penicillin-streptomycin (P/S) in presence of 1 μg/ml puromycin and 250 μg/ml G418. iSLK stable cell lines carrying KSHV Bac16 expressing RFP-LANA were cultured in iSLK-growth medium with additional 1200 μg/ml Hygromycin B. Human TIVE and L1T3/mSLK cells were gifts from Dirk P. Dittmer, University of North Carolina [15]. STR analysis [16] of L1T3 and L1T4 indicates that these cells are most closely related to SLK/Caki-1 cells. TIVE, KSHV-TIVE and BAC16 (TIVE-BAC16-LANA WT) cells were cultured in complete growth Medium199 with 20% FBS, 1% P/S and supplemented with 30 mg bECGF (Sigma, E2759). L1T4 cells were generated after an additional passage of L1T3 cells in mouse xenografts. L1T3 and L1T4 cells were cultured in DMEM with 10% FBS and 1% P/S. All cell lines were cultured at 37 °C, 5% $CO_2$.

### 2.3. Immunohistochemistry

Formalin-fixed, paraffin-embedded (FFPE) human tissue were divided into 4-μm sections. Slides were deparaffinized and rehydrated by means of standard xylene and ethanol washes. Endogenous peroxidase activity was blocked using a 3% $H_2O_2$, and antigen retrieval was performed in sodium citrate buffer, pH 6.0, in 98°C-steamer for 20 min. The slides were incubated with 0.3% TX-100 in PBS for 15 min and washed with PBST 10 min. Slides were blocked with 2.5% normal horse or goat serum (Vector Laboratories, 3022). The primary antibodies were diluted in green diluent (Biocare DaVinci, PD900 M) and incubated overnight at 4 °C: rat anti-LANA HHV8 [LN53] 1/50 (Abcam, ab-4103), rabbit iNOS 1/600 (Invitrogen, PA1-036), rabbit Nitrotyrosine Sigma 1/300 (NO409). The slides were washed with PBST and incubated 30 min with secondary antibodies: anti-rat (Vector, 30033) or anti-rabbit (Vector, 30026) polymer for HRP. DAB or AEC substrates and hematoxylin were used for chromogen deposition and counterstaining, respectively.

### 2.4. Immunofluorescent IHC (IF-IHC)

The slides with FFPE human tissue sections were deparaffinized, rehydrated and treated with sodium citrate pH 6.0, as described above. After washing with PBST, the slides were blocked with 4% BSA for 30 min and incubated with primary antibodies in blocking solution for 2 h, at RT. The antibodies were used: rat anti-LANA HHV8 [LN53] 1/200 (Abcam, ab-4103), rabbit anti-iNOS 1/100 (Invitrogen, PA1-036), rabbit anti-Nitrotyrosine Sigma 1/300 (NO409). After washing the slides were further incubated with fluorescence-conjugated secondary antibodies (Alexa Fluor, Invitrogen) in blocking solution for 1h, counterstained with DAPI and mounted in SlowFade Gold mounting solution (Life Technologies). Images were acquired with a Nikon 80i Upright Microscope (Nikon Instruments) at 60X or 100X lens using Nikon ImagePro Plus software (Media Cybernetics) and Adobe Photoshop CS6/2022 for image capture and processing.

### 2.5. Immunofluorescences on cell culture slides (IF)

For IF on cell culture we used our standard protocol (16, 17). Briefly, $1 \times 10^5$ cells were plated on glass coverslips in 24-well plate. Cells were washed with PBS and fixed for 15 min with 2% paraformaldehyde (Electron Microscopy Sciences) in PBS, washed twice with PBS and permeabilized with 0.3% TritonX-100 (Sigma) in PBS. All procedures were performed at room temperature. After washing with PBS, slides were incubated in blocking solution (0.2% fish gelatin, 0.5% BSA in PBS) for 30 min. Primary antibodies were diluted in blocking solution and applied on cells for 1h followed with PBS washing. Cells were further incubated with fluorescence-conjugated secondary antibodies (Invitrogen) in blocking solution for 1h, counterstained with DAPI and mounted in SlowFade Gold mounting solution (LifeTechnologies). Images were acquired with a Nikon 80i Upright Microscope (Nikon Instruments) at 60X or 100X lens using Nikon ImagePro Plus software (Media Cybernetics) and Adobe Photoshop CS6/or 2022 for image capture and processing.

### 2.6. Image quantification

Foci and colocalization was determined and quantified with Nikon NIS-Elements AR software, version 5.02 using the Bright Spot Detection Tool. For each detected nuclear body, a 1 μm circular binary outline is stored. For the detected objects, the growing feature adjusted to match the object's shape. Images acquired with the Nikon Upright Microscope utilized the Image-Pro Plus 7.1 software with saturation and exposure time tools to limit signal saturation. ImageJ 1.49 processing program

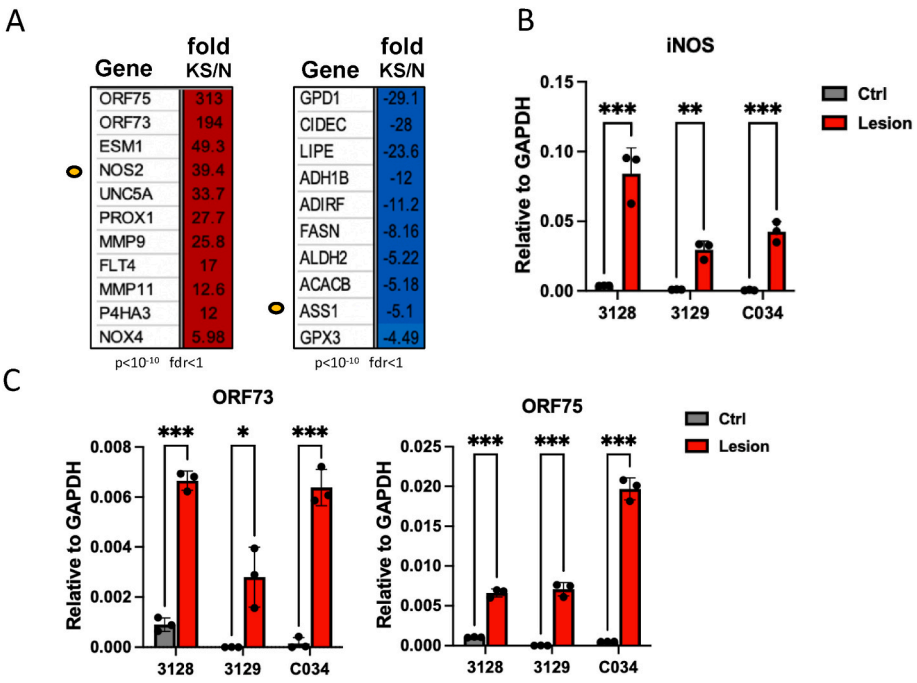


**Fig. 1. iNOS is expressed at high-levels in KS. A.** Analysis of KS transcriptomics (NCBI GEO GSE147704) reveals NOS2/iNOS is among the most up-regulated gene transcripts in KS lesions. Strongly down-regulated genes are also indicated. **B–C.** RT-qPCR for control skin (Ctrl, grey) or KS lesion (Lesion, red) for patient samples 3128, 3129, C034. Primers specific for iNOS, ORF75, and were analyzed by ΔΔCT method relative to GAPDH. Error bars are standard deviation from mean. *p < .05, **p < .01, ****p < .001 using 2way ANOVA with Fisher's Least Significant Difference test. (For interpretation of the references to colour in this figure legend, the reader is referred to the Web version of this article.)

was used to count only NBs that were not overexposed. The number of cells for quantifications was taken from 300 to 600 total.

### 2.7. Western blot

Cells were collected in RIPA buffer (50 mM Tris-HCl pH 8.0, 150 mM NaCl, 1% NP-40, 0.5% Sodium deoxycholate, 0.1% SDS, 1 mM EDTA). Equal amounts of protein extracts were resolved in 8–16% Tris-Glycine gels and then transferred onto PVDF membrane followed with specific antibodies application. Antibody signal was detected using Luminata HRP detection reagent (Millipore) and Luminescent Imager 680 (Amersham Biosciences). Antibodies were used: rat anti-LANA HHV8 [LN53] 1/1000 (Abcam, ab4103), rabbit anti-iNOS 1/300 (NOVUS, NB300-605), mouse anti-ORF45 (provided by Yan Yuan, UPENN), mouse anti-b-Actin-HRP 1/50.000 (Sigma, A23852).

### 2.8. RNA extraction and RT-qPCR

RNA was extracted from the cells using the RNeasy kit (Qiagen, 74106).

Reverse transcription was carried out on equal amounts of DNase-treated RNA using SuperScriptIV reverse transcriptase (Invitrogen), random priming mix (New England Biolabs), and RNase inhibitor (New England Biolabs) following the manufacturer's instructions. qPCR was performed with Power SYBR green 2X PCR mastermix with primers (Supplementary Table 1). Data was normalized to GAPDH or GUSB as indicated. Statistical significance of mean differences was determined by two-tailed *t*-test. Primers used in this study (Supplementary Table 1).

### 2.9. Mouse studies

*Ethics Statement:* All animal experiments were conducted under the Wistar Institute's approved Institutional Animal Care and Use Committee Protocol #201158 in accordance with the Committee for the Purpose of Control and Supervision of Experiments on Animals guidelines for animal experimentation. All mice in this study were managed in accordance with the NIH Office of Laboratory Animal Welfare: "PHS Policy on the Humane Care and Use of Research Animals"; the recommendations of the American Association for Accreditation of Laboratory Animal Care (AAALAC).

*Mice:* NSG mice (NOD.Cg-*Prkdc*$^{scid}$ *Il2rg*$^{tm1Wjl}$/SzJ) were bred in-house at The Wistar Institute under protocol #112092. Mice were enrolled at 6–8 weeks of age and housed in micro-isolator cages in a designated, specific pathogen-free facility where they were fed sterile food and water *ad libitum*. Mice were euthanized via $CO_2$ administration according to AALAC euthanasia guidelines.

*Tumor Implantation, Grouping, and Equalization*: Mice (five males and five females per treatment group) were engrafted with a cell suspension (>98% viability) of $1 \times 10^6$ L1T3 cells resuspended in 1X PBS, pH 7.4 and maintained on ice. Animals were weighed three-times per week and monitored daily.

*L-NMMA Formulation and Treatment Schedule*: L-NMMA resuspended in phosphate buffered saline (PBS). The vehicle control comprised PBS without compound. L-NMMA was administered q. d., i. p.at 25 mg/kg in a dose volume of 10 ml/kg body weight.

### 2.10. RNA-seq from L1T3 tumors

Tumor pieces (approximately 2–4 $mm^3$) were dissected and resuspended in lysis buffer (Qiagen, Germany) before homogenization with the TissueLyser II (Qiagen, Germany). Tissue was further homogenized using a QIAshredder (Qiagen, Germany) spin-column to reduce viscosity. Total RNA was isolated from homogenized tumor lysate using RNeasy Mini Kit (Qiagen, Germany). DNA was removed using on column deoxyribonuclease digestion following manufacturer's protocol (Qiagen, Germany). RNA samples were submitted to the Wistar Institute genomics core and assessed for RNA quality using the TapeStation (Agilent Technologies, Santa Clara, CA). Samples with RNA integrity (RIN) value greater than 8.5 were further subject to library preparation using the ScriptSeq RNA-seq library preparation kit (Lexogen). Sequencing was performed with an Illumina NextSeq 500 system in high-output mode to generate ~$4 \times 10^8$ read ($1 \times 75$ bp) across 12 multiplexed and pooled samples.

RNA-seq data was aligned using STAR algorithm [17] against hg19 human genome version and RSEM v1.2.12 software [18] was used to estimate read counts and RPKM values using gene information from mouse Ensemble transcriptome. Raw counts were used to estimate significance of differential expression difference between two experimental

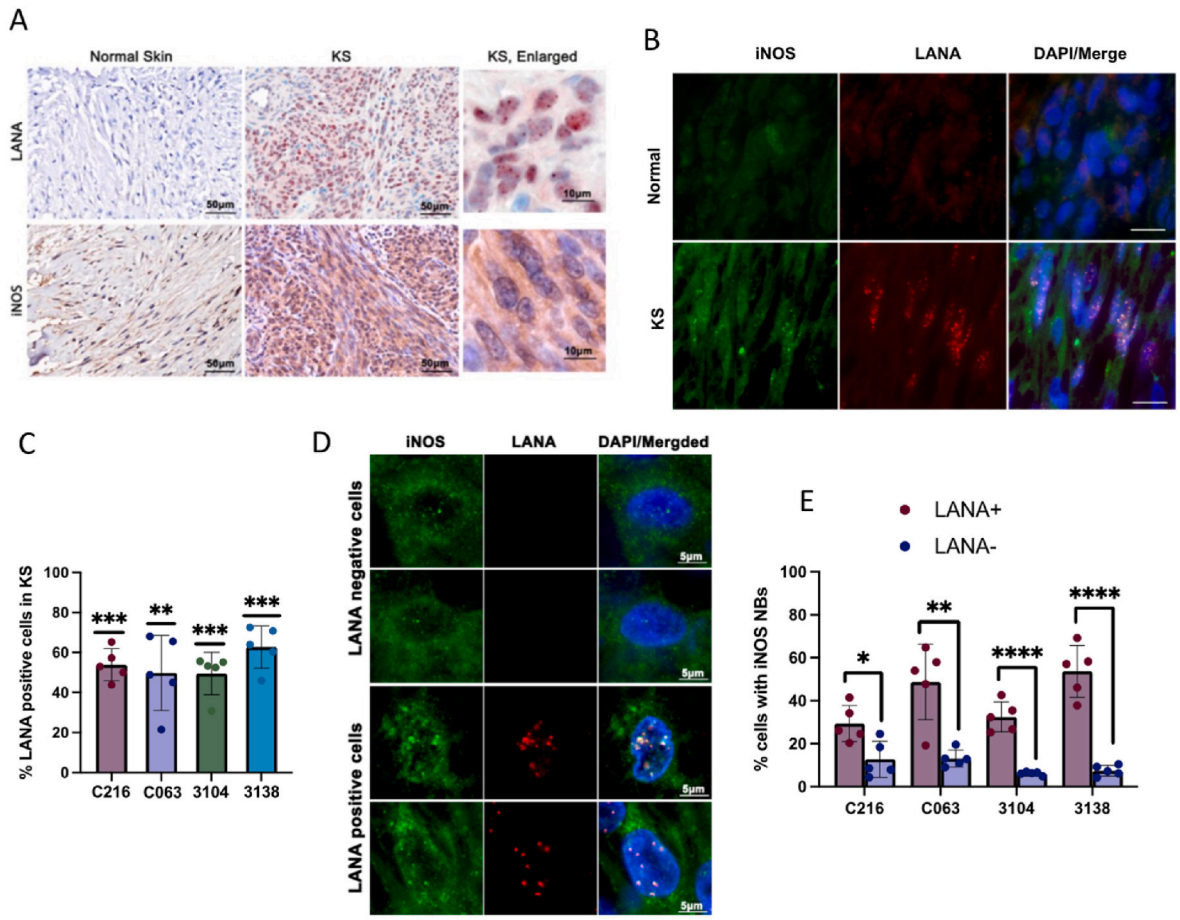


**Fig. 2. iNOS is enriched in LANA$^+$ KS tumor cells. A.** IHC of normal skin (left) or KS tumor (right) tissue sections stained with anti-LANA (top) or anti-iNOS (bottom). Enlarged image of KS samples (right panels). **B.** IF of normal skin (top) or KS tumor (bottom) with antibodies for iNOS (green), LANA (red), or DAPI (blue)/merge. Scale bar = 10 μm. **C.** Quantification of the percentage of LANA$^+$ cells in sections examined from patient biopsy samples. **D.** IF of LANA negative and LANA positive nuclei from KS lesions showing iNOS (green) and LANA (red), and DAPI/merge. **E.** Quantification of IF images represented in panel D, for four different patient biopsies. Each dot represents the mean value for each sample. Mean values were measured by manual counting from five different regions of the histological section. Percent cells with iNOS signals were scored for their colocalization with LANA$^+$ or LANA$^-$ cells. *p < .05, **p < .01, ****p < .0051 one-way ANOVA (C), and Mann-Whitney, unpaired *U* test (E). (For interpretation of the references to colour in this figure legend, the reader is referred to the Web version of this article.)

groups using DESeq2 [19]. Overall gene expression changes were considered significant if passed FDR<5% threshold unless stated otherwise. Gene set enrichment analysis was done using QIAGEN's Ingenuity® Pathway Analysis software (IPA, QIAGEN Redwood City,www.qiagen.com/ingenuity) using "Canonical pathways" option. Top results ranked by FDR were reported. Additional enrichment analysis was performed with GSEA algorithm [20] using Hallmark pathway MSigDB [21] categories and FDR<5% results were reported.

### 2.11. Data availability

RNA-seq data for L1T3 tumors treated with L-NMMA or vehicle control has been deposited in NCBI GEO under accession number GSE222527.

## 3. Results

### 3.1. iNOS is highly expressed in KS tumors

Previously published RNA-seq transcriptomics from KS tumor samples identified numerous genes differentially regulated in KS relative to control skin (NCBI GEO GSE147704) [5,6]. We searched for genes that were highly upregulated in KS lesions relative to control and encoded potential drug targets. We identified NOS2, a well-characterized druggable enzyme that is consistently up-regulated in KS tumors relative to controls (mean upregulation 30 fold, p value < .001, for n = 24 samples) (Fig. 1A). To validate RNA-seq, we assayed paired KS lesions and control skin from 3 different patients by RT-qPCR (Fig. 1B–C). Consistent with RNA-seq data, we found that all three patients (3128, 3129, C034) had significant enrichment of iNOS RNA in lesions relative to control (Fig. 1B). As expected, each of these biopsies were enriched for viral genes ORF73/LANA and ORF75 (Fig. 1C). These findings suggest that tumor biopsies from KS lesions are consistently enriched in iNOS and KS gene expression.

### 3.2. iNOS is expressed in LANA$^+$ cells and throughout KS tumors

To better understand the expression pattern of iNOS in KS tumor tissue, we performed IHC and IF-HC using antibodies to iNOS and LANA (Fig. 2). We compared KS lesions with normal skin in four different patient paired biopsies. iNOS was generally detected throughout tumor lesion and enriched relative to normal skin control. While all KS lesions were found to contain LANA expressing cells, the percentage of LANA positive cells varied among tumor samples and sections. Overall, we detected LANA in ~50% of the cells examined in these tumor samples (Fig. 2C, Supplemental Fig. S1). We then asked whether iNOS signal

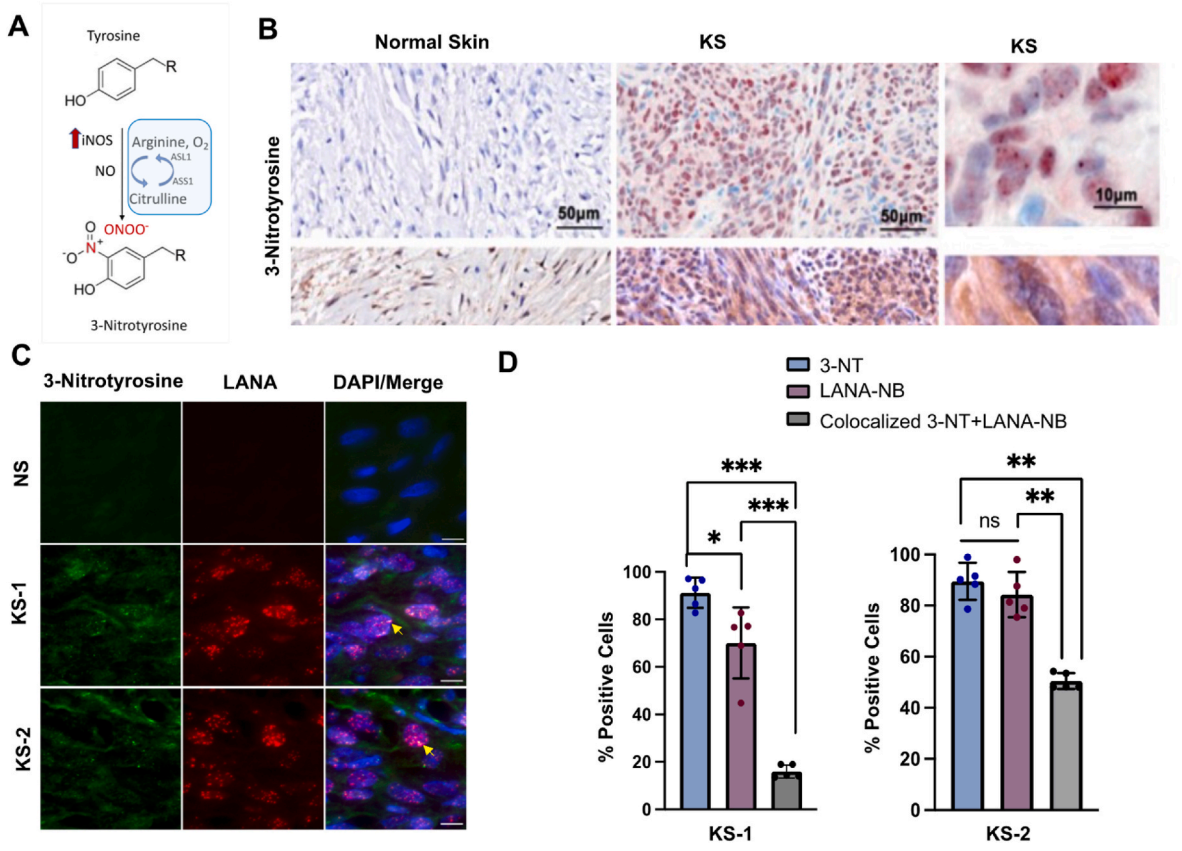


**Fig. 3. Detection of 3-nitrotyrosin in KS tissue sections. A**. Schematic of 3-nitrotyrosine formation by iNOS and NO metabolism. **B.** IF images of 3-nitrotyrosine (green) or LANA (red) and merged with DAPI (blue) in normal skin (top panel) or KS lesions KS-1 (KSC3094) or KS-2 (KS2005961) (bottom panels). Yellow arrow indicates colocalization of 3-nitrotyrosine with LANA-NB. **C.** Quantification of percent KS cells with IF signal for LANA-NBs, 3-nitrotyrosine (3-NT) and colocalization of 3-NT with n > 1 LANA-NBs. **p < .01, ***p < .005, Mann-Whitney, unpaired *U* test. Scale bar = 10 μm. (For interpretation of the references to colour in this figure legend, the reader is referred to the Web version of this article.)

localized to cells that also express LANA. Higher-resolution IF on FFPE tumor and normal skin samples revealed that iNOS signal was detected more frequently and intensely in LANA-positive relative to LANA-negative cells (Fig. 2D and E). iNOS signal was mostly present in perinuclear and cytoplasmic aggregates, but was also found to occasionally colocalize with LANA nuclear bodies (Fig. 2D).

### 3.3. Enrichment of nitrotyrosine in LANA positive KS tumor cells

High levels of iNOS protein can correlate with NO-associated protein modifications such as 3-nitrotyrosine (Fig. 3A) [22]. Therefore, we examined whether KS tumor sections were enriched for 3-nitrotyrosine signal [23]. IHC analysis with an antibody specific for 3′-nitrotyrosine indicated enrichment in KS relative to normal skin (Fig. 3B and Supplemental Fig. S2). Higher resolution IFC revealed that 3-nitrotyrosine signal was enriched in LANA positive cells and form nuclear foci that occasionally colocalize with LANA nuclear bodies (NBs) (Fig. 3C and D). LANA-NBs are indicative of LANA bound to KSHV episomes [24,25]. We found that cells with 3-nitrotyrosine colocalizing with LANA-NBs occur at frequency ranging from 17% to 50% (Fig. 3D). These findings suggest that KS lesions are enriched for 3-nitrotyrosine and that 3′-nitrotyrosine frequently colocalizes with LANA-NBs.

### 3.4. iNOS is highly expressed in L1T tumor models

We next investigated cells and conditions where KSHV infection could induce iNOS in vitro. We were unable to demonstrate consistent induction of iNOS by KSHV-infection in commonly used cell lines, including SLK, HUVEC, LECs, MSCs, and TIVE cells (**data not shown**). We then examined iNOS expression in the mouse adapted SLK cell line L1T/mSLK (referred to here as L1T3 and L1T4) selected for tumor formation in mouse xenografts [15,26] (Fig. 4). We assayed the expression iNOS and KSHV proteins LANA and ORF45 by Western blot in uninfected TIVE, L1T3 cells passaged in 2D culture, and L1T3 cells derived directly from mouse tumor (Fig. 4A). We found that iNOS expression was significantly increased in L1T3 cells and tumors relative to uninfected TIVE cells. We also found that LANA and ORF45 were expressed at higher levels in tumors, relative to L1T3 cell cultures or TIVE cells. We next assayed RNA expression by RT-qPCR (Fig. 4C) comparing uninfected TIVE with freshly generated L1T3 cells passaged in 2D culture, and two freshly isolated tumors, Tumor-1 grown for 1 month, and Tumor-2 grown for 2.5 months in mouse. We found that NOS2 was elevated in L1T3 cells and tumors relative to TIVE cells. This was confirmed with two different primer pairs for NOS2. Interestingly, the older tumor 2 showed significantly more NOS2 expression relative to the younger tumor 1. We also found that MMP11, which is significantly upregulated in KS tumors, was strongly (>10 fold) upregulated in tumor 2 relative to tumor1 and 2D cell cultures. KSHV genes ORF71, ORF72, LANA were expressed similarly in all L1T3 cells, Tumor-1 (harvested at 1 month, size = 552.35 $mm^3$) and Tumor-2 (harvested at 2 months, size = 1889.19 $mm^3$), and not detected in uninfected TIVE cells (Fig. 4C, lower panel). Interestingly, KSHV genes associated with lytic cycle, such as ORF50, ORF45 and PAN, were highly upregulated in tumor 2, similar to MMP11 and iNOS, and consistent with Western blotting data shown in Fig. 4A. These findings suggest that L1T model may be useful for investigating iNOS, and that lytic cycle gene expression may be an important component of iNOS activation and KS transcription control. To further assess the L1T3 model, we assayed iNOS and nitrotyrosine

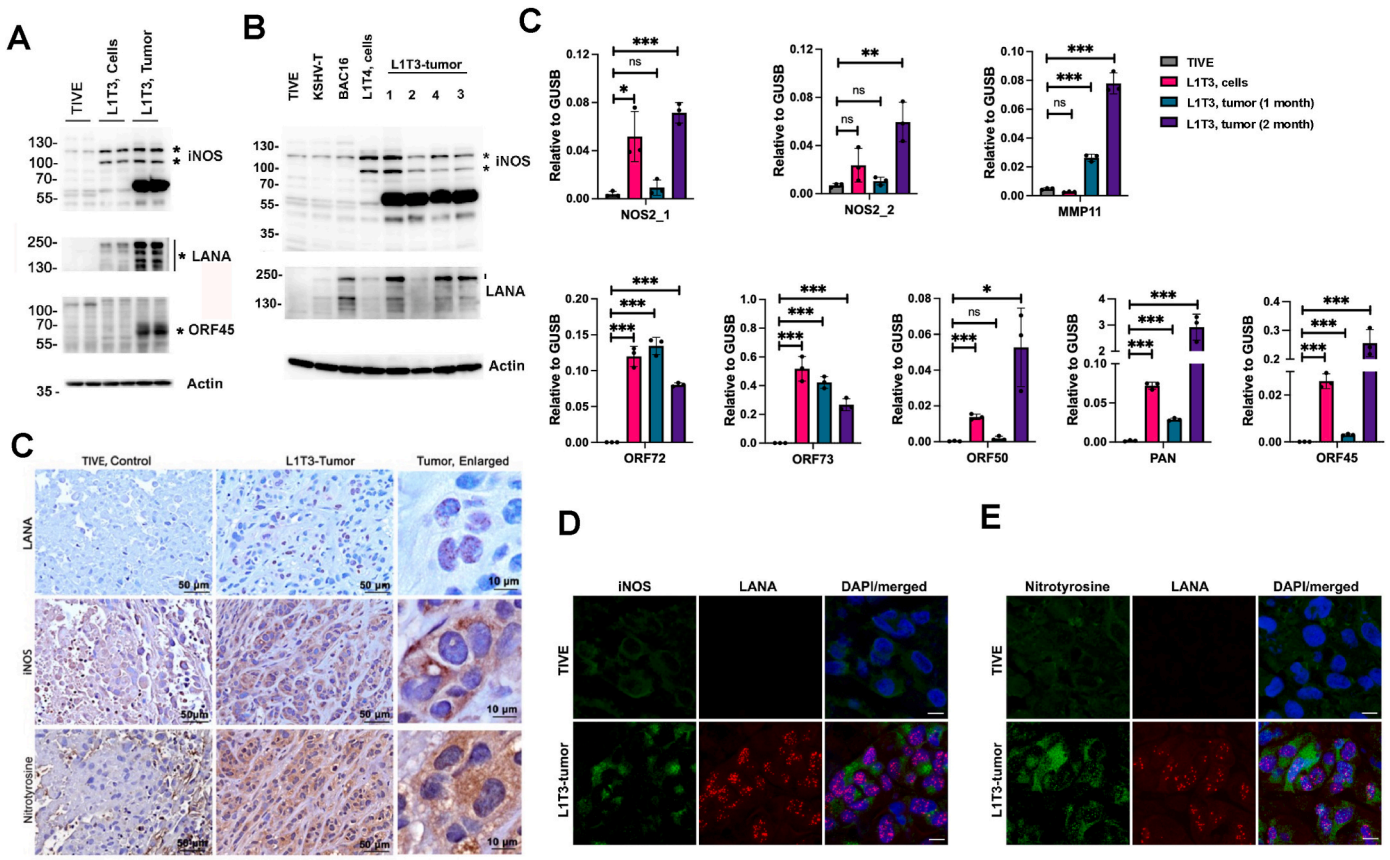


**Fig. 4. iNOS and nitrotyrosine expression in L1T3 tumor model. A.** Western blot of TIVE, L1T3 cells, and L1T3 mouse xenograft tumors assayed for iNOS, LANA, ORF45, and Actin. Molecular weight markers indicated to the left. **B.** Western blot of TIVE, KSHV-TIVE (KSHV-T), TIVE-BAC16-LANA-WT (BAC16), L1T4 cell lines and L1T3 xenograft tumors 1–4 assayed for iNOS, LANA, and Actin. Tumors 1, 3 and 4 harvested at 1 month. Tumor 2 harvested at 2 months. **C.** RT-qPCR for two different primer sets of iNOS (NOS2_1, NOS2_2), MMP11, ORF72, LANA, ORF50, PAN gene transcripts in RNA isolated from TIVE, L1T3 cells, and L1T3 tumors taken at 1 month (Tumor 1) or 2 months (Tumor 2). *p < .05, **p < .01, ***p < .001, or ns (not significant), p values determined by two-tailed *t*-test. **D.** IHC of TIVE xenograft control (left) or L1T3 tumors (right, enlarged image far right) stained with LANA (top), iNOS (middle) or 3-nitrotyrosine (bottom). **E.** IF of TIVE xenograft control (top) or L1T3 tumor (bottom) imaged with iNOS (green) or LANA (red), and DAPI (blue)/merge. **F.** Same as in D, except 3-nitrotyrosine (green). Scale bar = 10 μm. (For interpretation of the references to colour in this figure legend, the reader is referred to the Web version of this article.)

expression by IHC (Fig. 4D) and IF (Fig. 4E). We found that L1T3 tumors have similar levels of LANA, iNOS and nitrotyrosine that were observed in KS tumor tissue (Fig. 4D). Furthermore, we found that iNOS and nitrotyrosine were enriched in cells that express LANA. These finding suggest that L1T3 cells recapitulate key aspects of KS tumors.

### *3.5. iNOS inhibitor L-NMMA reduces L1T3 tumor growth and viral gene expression in mouse tumor model*

To investigate whether iNOS functionally contributes to L1T3 tumor growth, we assayed the effects of the iNOS small molecule inhibitor L-NMMA ($N^G$-methyl L-arginine) on L1T3 tumor growth in mice (Fig. 5). L1T3 tumors were engrafted in a cohort of 10 mice and then treated with 25 mg/kg ip,qd or with vehicle control. Tumor size was assayed by caliper 3 days per week for a total of 22 days. We found that treatment of mice with L-NMMA resulted in a ~4-fold reduction in tumor growth (Fig. 5A). Mice did not lose weight from L-NMMA treatment suggesting that the effects were not due to general toxicity (Fig. 5B). We also assayed the effects of L-NMMA on tumor by IFA (Supplementary Figs. S3 and S4). We found no significant change in treated vs untreated, although there was a trend for increased iNOS signal after treatment, potentially due to L-NMMA inhibition and feedback upregulation (Fig. S4). We did not observe any differences in tumor response between male and female mice.

To better assess the mechanism of action of L-NMMA tumor growth inhibition, we assayed viral gene expression by RT-qPCR (Fig. 5C) from tumors treated with vehicle or L-NMMA (25 mg/kg) at day 25, as in Fig. 5A. We found that L-NMMA treated tumors had reduced (~3–4 fold) expression for all KSHV genes tested, including LANA, ORF75, ORF45 and ORF50, relative to cellular GUSB (Fig. 5C). We assessed potential changes in cellular gene expression by RNA-seq analysis comparing treated to untreated tumor samples. RNA-seq revealed numerous significant changes in gene expression (Fig. 5D). Among the most statistically significant (lowest FDR values) were up-regulation of HINT1, TYMS, SNPG and down regulation of EIF3C, VEGFA, and ENO2. Ingenuity Pathway Analysis (IPA) identified oxidative phosphorylation, mitochondrial dysfunction, and Sumoylation among the most significantly affected pathways (FDR<5%) (Fig. 5E). Significant enrichment of HALLMARK pathways based on GSEA data analysis identified oxidative phosphorylation, Myc targets and E2F targets among the top gene categories (Fig. 5F). Taken together, these finding indicate that the L-NMMA reduces L1T3 tumor formation and KSHV gene expression through a mechanism perturbing oxidative phosphorylation, mitochondrial function and cell cycle control (e.g. Myc and E2F targets).

## 4. Discussion

In this study, we show that KSHV tumors express high levels of iNOS, a druggable enzyme with complex functions in endothelial and immune cell biology. We demonstrate by RNA-seq, RT-qPCR, IHC and IF that

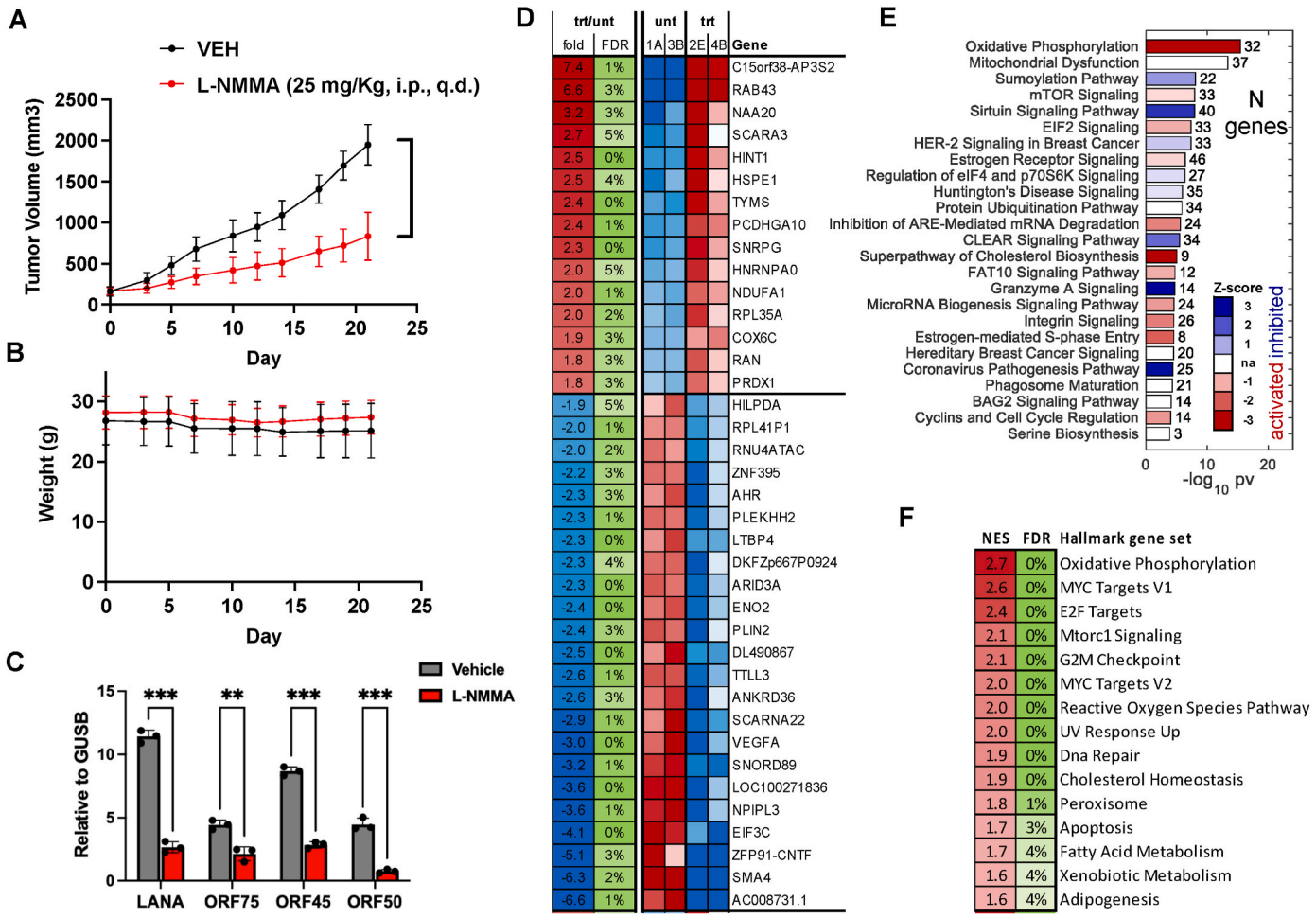


**Fig. 5. iNOS inhibitor L-NMMA inhibits L1T3 growth in mouse xenograft. A.** Mouse xenografts of L1T3 were normalized into groups (n = 10/group) when tumors reached 100 $mm^3$ and treated daily with L-NMMA (25 mg/kg) (red) or vehicle control (black) i. p. **B.** Tumor volume(top) and body weight (bottom) were measured three times per week for 23 days. ****p < .0001 ANOVA followed by Tukey T-test and multiple comparison test. **C.** RNA-qPCR analysis tumor samples from mice treated with vehicle or L-NMMA as described in panel A, tested for LANA, ORF75, ORF45 or ORF50 relative to GUSB. ***p < .001, **p < .01, using two-tailed student t-test. **D.** RNA-seq analysis from tumors samples (n = 2) for both vehicle or L-NMMA treated tumors. Heat map of top significantly changed genes (all pass FDR<5%). **E.** Top 25 (all pass FDR<5%) significantly affected pathways determined by IPA. **F.** FDR<5% HALLMARK sets enriched as identified by GSEA. NES = normalized enrichment score. (For interpretation of the references to colour in this figure legend, the reader is referred to the Web version of this article.)

iNOS is upregulated in LANA-positive KS tumor cells. RT-qPCR analysis of KS tumor sections suggests that iNOS expression correlates with KSHV lytic gene activity. We also found that the nitric oxide byproduct 3-nitrotyrosine was elevated in IHC and IF of KS tumors with partial colocalization with LANA-NBs. The KSHV-associated increase in iNOS activity could be partially recapitulated in tumor-derived L1T3 models of KS, where KSHV infected cells have been selected for growth as tumor xenografts in mice. In this model, we observed high levels of iNOS and 3-nitrotyrosine, and some correlation with KSHV lytic gene expression in long-term (~2 month) tumors in mice. Finally, we show that a small molecule inhibitor of NOS can reduce L1T3 tumor growth in vivo, and that this correlates with loss of KSHV gene expression and perturbation of oxidative phosphorylation and mitochondrial dysfunction. These findings suggest that iNOS may be an attractive target for therapeutic intervention in KS.

iNOS and NO have been previously implicated in KSHV oncogenesis [8,27]. Early studies identified iNOS protein and NOS activity in KS tumor sections [7]. More recent studies demonstrated elevated levels of NO in KSHV-transformed rat embryonic metanephric mesenchymal cells (KMM) [8]. In the KMM model, and both iNOS and ASS1 were highly upregulated, and shown to be important for activation of STAT3 [8]. A related study on primary human B-cells found that KSHV infection increased NO production, and that exogenous NO donor S-nitroso-N-acetyl-D, L-penicillamine (SNAP) was important for KSHV lytic replication [27]. Inhibition of NOS by L-NAME reduced virion production [27]. We observed that ASS1 is down-regulated in KS tumor transcriptomics (Fig. 1A). This suggests that mechanism regulating NO production by iNOS may be different in KS tumors relative to the KMM model. KSHV infection induces hypoxia and angiogenic response in several cell culture models, including HUVEC [28,29] and SLK cells [30], but these failed to show an increase in iNOS in 2D models. We were also unable to show that iNOS induction under hypoxia conditions in 2D cell culture models grown in low $O_2$ (2%) nor treatment with hypoxia mimic $CoCl_2$.

iNOS has a complex role in oxygen metabolism and signaling. NO diffusion can also promote angiogenesis, by activation of cGMP resulting in the activation of HIF1a and VEGF pathway signaling [31]. Very high levels of NO generated by iNOS can also prevent the stabilization of HIF1A even during hypoxia by competing with $O_2$ and reversing mitochondrial respiration (fumarate to succinate) [32,33]. KS transcriptomics further support changes in mitochondrial function. High levels of NO produced by iNOS are known to inhibit cytochrome C oxidase and permanently damage mitochondria [31]. NO production can also lead to nitration products, such as S-nitrosylation of HIF1-α, 3-nitrotyrosines, and nitration of unsaturated fatty acids to modulate nitro-lipids [31]. We observed high-levels of 3-nitrotyrosine in IHC and

IF analysis of KS and L1T3 tumors sections, including a high-frequency of colocalization with LANA-NBs. Thus, iNOS may affect tumorigenesis through protein and lipid modification, as well as through changes in mitochondrial metabolism.

It is also possible that iNOS is expressed in non-KSHV infected tumor-associated cells, such as macrophages or plasma B-cells. Our RNA-seq did not find strong evidence of macrophage infiltration, but B-cell signatures, including high levels of IgG were observed. This is consistent with a recent study showing by IF and IHC that macrophages and T-cells tend not to colocalize with LANA$^+$ KS cells [34]. iNOS can be expressed in activated plasma B-lymphocytes [35,36]. In macrophages, iNOS gene expression is regulated by gamma-interferon pathway, but the transcription control in tumor cells may depend on inflammatory cytokines and hypoxia [13,37]. We found that iNOS expression was most elevated in L1T3 tumors, especially after long-term culture, suggesting factors associated with an aging tumor microenvironment, such as hypoxia and nutrient deprivation, may be critical factors in the activation of iNOS in KS. Taken together, our data indicates that iNOS is highly expressed in KS tumors, and that this can be partly recapitulated in the L1T3 tumor model. Importantly, a small molecule inhibitor of iNOS was found to reduce L1T3 tumor growth in vivo. These findings suggest that iNOS may be an attractive target for small molecule therapy to treat KS.

## 5. Limitations of the study and conclusions

To date, no cell culture or tumor model completely recapitulates all aspects of KSHV-associated tumorigenesis relating to KS. The L1T3 tumor is a mouse adapted SLK/Caki-1 carcinoma cell infected with latent KSHV, and lacks endothelial features associated with KS tumors. Nevertheless, we found that L1T3 tumors expressed high levels of iNOS while most other KSVH cell lines did not, therefore making L1T3 a useful model for the study of iNOS in KS. We demonstrate that iNOS/NOS2 and iNOS by-product 3-nitrotyrosine are elevated in KS tumor cells that express KSHV-encoded LANA. We show that iNOS is elevated in KSHV$^+$ L1T3 tumor models and that a small molecule inhibitor of iNOS reduces tumor growth. These findings identify iNOS as a potential target for treatment of KS and an animal model to test its efficacy and mechanism of action.

## Funding

This work was funded by RO1 CA117830 to PML, R50 CA211199 to AK, U54 CA221204 to CW, and R01 CA228178 to JW and CW.

## Author contributions

OV, SS, CV designed and performed experiments. ON, FYT, JTW, CW provided reagents, validation, and manuscript editing. AK analyzed genomic data and prepared figures. PML and OV designed experiments, provided funding, and prepared the manuscript.

## Author statement

Paul M. Lieberman discloses a financial conflict of interest as founder and advisor to Vironika LLC. No other others have any conflicts to disclose.

## Declaration of competing interest

The authors declare the following financial interests/personal relationships which may be considered as potential competing interests: Paul M. Lieberman is a founder and advisor to Vironika, LLC.

## Data availability

Data will be made available on request.

## Acknowledgements

We thank to F. Keeney of Wistar Imaging facility for help on imaging and analysis.

We thank to Fangping Chen of Wistar Histology facility for helping with FFPE, sectioning and IHC staining.

## Appendix A. Supplementary data

Supplementary data to this article can be found online at https://doi.org/10.1016/j.tvr.2023.200259.

## References

[1] R. Ramaswami, K. Lurain, R. Yarchoan, Oncologic treatment of HIV-associated Kaposi sarcoma 40 Years on, J. Clin. Oncol. 40 (3) (2022) 294–306.
[2] Y. Chang, P. Moore, Twenty years of KSHV, Viruses 6 (11) (2014) 4258–4264.
[3] E. Cesarman, et al., Kaposi sarcoma, Nat. Rev. Dis. Prim. 5 (1) (2019) 9.
[4] M.A. Valantin, et al., Therapeutic Perspectives in the systemic treatment of Kaposi's sarcoma, Cancers 14 (3) (2022).
[5] S.J. Lidenge, et al., Comparative transcriptome analysis of endemic and epidemic Kaposi's sarcoma (KS) lesions and the secondary role of HIV-1 in KS pathogenesis, PLoS Pathog. 16 (7) (2020) e1008681.
[6] F.Y. Tso, et al., RNA-Seq of Kaposi's sarcoma reveals alterations in glucose and lipid metabolism, PLoS Pathog. 14 (1) (2018) e1006844.
[7] W. Weninger, et al., Nitric oxide synthases in Kaposi's sarcoma are expressed predominantly by vessels and tissue macrophages, Lab. Invest. 78 (8) (1998) 949–955.
[8] T. Li, et al., Oncogenic Kaposi's sarcoma-associated herpesvirus upregulates Argininosuccinate synthase 1, a rate-limiting enzyme of the Citrulline-nitric oxide cycle, to activate the STAT3 pathway and promote growth Transformation, J. Virol. 93 (4) (2019).
[9] F. Vannini, K. Kashfi, N. Nath, The dual role of iNOS in cancer, Redox Biol. 6 (2015) 334–343.
[10] K. Kashfi, J. Kannikal, N. Nath, Macrophage reprogramming and cancer therapeutics: role of iNOS-derived NO, Cells 10 (11) (2021).
[11] F.H. Khan, et al., The role of nitric oxide in cancer: master regulator or NOt? Int. J. Mol. Sci. 21 (24) (2020).
[12] J. Dong, M. Cheng, H. Sun, Function of inducible nitric oxide synthase in the regulation of cervical cancer cell proliferation and the expression of vascular endothelial growth factor, Mol. Med. Rep. 9 (2) (2014) 583–589.
[13] H.S. Jeffrey Man, A.K. Tsui, P.A. Marsden, Nitric oxide and hypoxia signaling, Vitam. Horm. 96 (2014) 161–192.
[14] J. Myoung, D. Ganem, Generation of a doxycycline-inducible KSHV producer cell line of endothelial origin: maintenance of tight latency with efficient reactivation upon induction, J. Virol Methods 174 (1–2) (2011) 12–21.
[15] D. Roy, et al., mTOR inhibitors block Kaposi sarcoma growth by inhibiting essential autocrine growth factors and tumor angiogenesis, Cancer Res. 73 (7) (2013) 2235–2246.
[16] W.G. Dirks, H.G. Drexler, STR DNA typing of human cell lines: detection of intra- and interspecies cross-contamination, Methods Mol. Biol. 946 (2013) 27–38.
[17] A. Dobin, et al., STAR: ultrafast universal RNA-seq aligner, Bioinformatics 29 (1) (2013) 15–21.
[18] B. Li, C.N. Dewey, RSEM: accurate transcript quantification from RNA-Seq data with or without a reference genome, BMC Bioinf. 12 (2011) 323.
[19] M.I. Love, W. Huber, S. Anders, Moderated estimation of fold change and dispersion for RNA-seq data with DESeq2, Genome Biol. 15 (12) (2014) 550.
[20] D.A. Barbie, et al., Systematic RNA interference reveals that oncogenic KRAS-driven cancers require TBK1, Nature 462 (7269) (2009) 108–112.
[21] A. Liberzon, et al., The Molecular Signatures Database (MSigDB) hallmark gene set collection, Cell Syst. 1 (6) (2015) 417–425.
[22] N. Campolo, et al., 3-Nitrotyrosine and related derivatives in proteins: precursors, radical intermediates and impact in function, Essays Biochem. 64 (1) (2020) 111–133.
[23] H. Maeda, T. Akaike, Nitric oxide and oxygen radicals in infection, inflammation, and cancer, Biochemistry (Mosc.) 63 (7) (1998) 854–865.
[24] O. Vladimirova, et al., Phase separation and DAXX redistribution contribute to LANA nuclear body and KSHV genome dynamics during latency and reactivation, PLoS Pathog. 17 (1) (2021) e1009231.
[25] A. De Leo, et al., LANA oligomeric architecture is essential for KSHV nuclear body formation and viral genome maintenance during latency, PLoS Pathog. 15 (1) (2019) e1007489.
[26] A.B. Eason, et al., DLX1008 (brolucizumab), a single-chain anti-VEGF-A antibody fragment with low picomolar affinity, leads to tumor involution in an in vivo model of Kaposi Sarcoma, PLoS One 15 (5) (2020) e0233116.
[27] A. Herrera-Ortiz, W. Meng, S.J. Gao, Nitric oxide is induced and required for efficient Kaposi's sarcoma-associated herpesvirus lytic replication, J. Med. Virol. 93 (11) (2021) 6323–6332.
[28] T. Ma, et al., KSHV induces aerobic glycolysis and angiogenesis through HIF-1-dependent upregulation of pyruvate kinase 2 in Kaposi's sarcoma, Angiogenesis 18 (4) (2015) 477–488.

[29] B.C. Jham, et al., Amplification of the angiogenic signal through the activation of the TSC/mTOR/HIF axis by the KSHV vGPCR in Kaposi's sarcoma, PLoS One 6 (4) (2011), e19103.
[30] C. Viollet, et al., RNA Sequencing reveals that Kaposi sarcoma-associated herpesvirus infection mimics hypoxia gene expression signature, PLoS Pathog. 13 (1) (2017) e1006143.
[31] J.O. Lundberg, E. Weitzberg, Nitric oxide signaling in health and disease, Cell 185 (16) (2022) 2853–2878.
[32] T. Hagen, et al., Redistribution of intracellular oxygen in hypoxia by nitric oxide: effect on HIF1alpha, Science 302 (5652) (2003) 1975–1978.
[33] U. Berchner-Pfannschmidt, et al., Oxygen-sensing under the influence of nitric oxide, Cell. Signal. 22 (3) (2010) 349–356.
[34] P. Julius, et al., Epstein-barr virus, but not human Papillomavirus, is associated with Preinvasive and invasive ocular Surface Squamous Neoplasias in Zambian patients, Front. Oncol. 12 (2022), 864066.
[35] M.N. Njau, J. Jacob, Inducible nitric oxide synthase is crucial for plasma cell survival, Nat. Immunol. 15 (3) (2014) 219–221.
[36] A.S. Saini, et al., Inducible nitric oxide synthase is a major intermediate in signaling pathways for the survival of plasma cells, Nat. Immunol. 15 (3) (2014) 275–282.
[37] M. Kielbik, I. Szulc-Kielbik, M. Klink, The potential role of iNOS in ovarian cancer progression and Chemoresistance, Int. J. Mol. Sci. 20 (7) (2019).